Extractable information capacity in sequential measurements metrology

Yaoling Yang [1,*] Victor Montenegro [1,2,†] and Abolfazl Bayat [1,2,‡]

[1]*Institute of Fundamental and Frontier Sciences, University of Electronic Science and Technology of China, Chengdu 611731, China*
[2]*Key Laboratory of Quantum Physics and Photonic Quantum Information, Ministry of Education, University of Electronic Science and Technology of China, Chengdu 611731, China*

The conventional formulation of quantum sensing is based on the assumption that the probe is reset to its initial state after each measurement. In a very distinct approach, one can also pursue a sequential measurement scheme in which time-consuming resetting is avoided. In this situation, every measurement outcome effectively comes from a different probe, yet is correlated with other data samples. Finding a proper description for the precision of sequential measurement sensing is very challenging as it requires the analysis of long sequences with exponentially large outcomes. Here, we develop a recursive formula and an efficient Monte Carlo approach to calculate the Fisher information, as a figure of merit for sensing precision, for arbitrary lengths of sequential measurements. Our results show that the value of the Fisher information initially increases nonlinearly with the number of measurements and then asymptotically saturates to a linear scaling. This transition, which fundamentally constrains the extractable information about the parameter of interest, is directly linked to the finite memory of the probe when it undergoes multiple sequential measurements. Based on these findings, we establish a figure of merit to determine the optimal measurement sequence length and exemplify our results in three different physical systems.

I. INTRODUCTION

Quantum probes exhibit unparalleled precision compared with their classical counterparts for a given resource [1]. The resource efficiency of quantum probes has been demonstrated through exploiting the superposition principle via Greenberger-Horne-Zeilinger-type entanglement [2–8], criticality in many-body systems [9–19], variational methods [20–22], adaptive [23–27] or continuous measurements [28–34], and Floquet dynamics [35,36], to name a few. In a general quantum sensing scenario, to estimate an unknown parameter λ encoded in the quantum state ρ_λ, one performs a measurement in a certain basis and then feeds the outcomes to a classifier. The precision is bounded through the Cramér-Rao inequality $\delta\lambda \geqslant 1/\sqrt{M\mathcal{F}_\lambda}$, where $\delta\lambda$ is the uncertainty in estimating λ, M is the number of trials, and $\mathcal{F}_\lambda$ is the Fisher information (FI) [37–41]. While classical sensors exhibit linear scaling of the FI with respect to a given resource (e.g., measurement time), quantum probes demonstrate greater resource efficiency, enabling the possibility of achieving superlinear behavior. The formulation of the Cramér-Rao inequality assumes the resetting of the probe after each measurement or equivalently using M identical probes at once. By

avoiding the time-consuming resetting procedure, the quantum state of the probe would be different for each data sample, implying the use of several nonidentical probes for sensing an unknown parameter. Therefore a question arises: How will the precision scale when measurements are performed sequentially without resetting the probe?

In many-body systems with partial accessibility, local measurements on a subsystem lead to a global wave function collapse, which has been the subject of intensive studies [42–54]. In the domain of quantum metrology, sequences of projective measurements followed by free evolution at regular time intervals have led to Hamiltonian identification [55] and sequential measurements sensing schemes [56–65] and even hint at quantum-enhanced sensitivity observed in short sequences that are computationally feasible [66,67]. Studying sequential measurements sensing schemes is typically limited to short lengths of measurement sequences. The limitation arises from the exponential growth of measurement outcomes with the number of measurement sequences. Indirect approaches, based on a functional of the measurement outcomes [56] or correlated stochastic processes [68], have been proposed to estimate sensing precision with a large number of sequential measurements. Interestingly, for short ($\sim$20) measurement sequences, it has been demonstrated that the FI increases superlinearly with the number of measurements [66,67], whereas the FI stemming from indirect methods scales linearly in the asymptotic limit of sequential measurements [56]. To reconcile this apparent discrepancy, an efficient approach to studying the FI for an arbitrary number of measurements is highly desirable.

In this paper, we develop a recursive formula and an efficient Monte Carlo approach to compute the FI for arbitrary

*yyaoling@std.uestc.edu.cn
†vmontenegro@uestc.edu.cn
‡abolfazl.bayat@uestc.edu.cn

lengths of measurement sequences. Our results show that the FI exhibits nonlinear growth in the beginning and asymptotically saturates to a linear function. Interestingly, this transition directly relates to the memory of an early state. In fact, the quantum probe retains only a finite memory of its initial state during multiple sequences of evolution and local projective measurements. Once the probe loses its memory, the FI grows linearly with additional measurements. This enables us to establish a figure of merit for determining the optimal reset point, maximizing the sensing protocol. To support our findings, we investigate three distinct physical systems in both closed and open quantum systems.

The rest of the paper is organized as follows: In Sec. II, we explain the general steps of the sequential measurements sensing protocol. In Sec. III, we introduce the Fisher information and derive a recursive formula to evaluate the Fisher information for an arbitrary number of measurements. To enable efficient simulations for a large number of measurement steps, we employ a Monte Carlo approach for this purpose. In Sec. IV, we investigate the probe's memory loss due to performing local measurements at regular time intervals. In Sec. V, we make use of the recursive Fisher information formalism developed herein to determine the maximum extractable information capacity of the probe in the limit of a large number of sequential measurements. In Sec. VI, we investigate the robustness of our numerical simulations. In Sec. VII, we examine the number of measurements and the total protocol time as sensing resources. Finally, in Sec. VIII, we present our concluding remarks. Appendixes A and B present the mathematical proof of the recursive Fisher information formula and the dynamics of the Jaynes-Cummings model under sequential measurements, respectively.

II. SEQUENTIAL MEASUREMENT SENSING PROTOCOL

Conventional sensing schemes typically rely on measurement outcomes with independent and identically distributed (i.i.d.) probability distributions. Hence, after measuring the probe, it is necessary to reset the sensing procedure to its exact initial quantum state in preparation for another round of measurements. These requirements may result in resource-demanding state preparation and time overhead due to unavoidable resetting procedures. On the other hand, sequential sensing schemes [56,66,67] utilize non-i.i.d. probability distributions constructed from consecutive measurements on the probe at regular intervals. Let us consider a probe initialized in a quantum state $\rho^{(1)}(0) = \rho_0$. The sequential sensing protocol is an iterative approach.

(i) The quantum probe $\rho^{(i)}(0)$ freely evolves to $\rho^{(i)}(\tau_i) = U_\lambda^{(i)} \rho^{(i)}(0) U_\lambda^{(i)\dagger}$ with a unitary time evolution operator $U_\lambda^{(i)}$.

(ii) At time τ_i a local positive operator-valued measure (POVM) $\{\Pi_{\gamma_i}\}$ with random outcome γ_i is performed on the probe, collapsing the state into

$$\rho^{(i+1)}(0) = \Pi_{\gamma_i} \rho^{(i)}(\tau_i) \Pi_{\gamma_i}^\dagger / p(\gamma_i), \tag{1}$$

where

$$p(\gamma_i) = \text{Tr}\big[\Pi_{\gamma_i} \rho^{(i)}(\tau_i) \Pi_{\gamma_i}^\dagger\big] \tag{2}$$

is the probability associated with γ_i at step i.

(iii) The outcome γ_i is recorded, and the new initial state $\rho^{(i+1)}(0)$ is replaced in step (i).

(iv) The above steps are repeated until n_{seq} measurement outcomes are consecutively obtained.

(v) After gathering a data sequence $\gamma = (\gamma_1, \ldots, \gamma_{n_{\text{seq}}})$, the probe is reset to ρ_0, and the process is repeated to generate a new trajectory.

In what follows, we study the above sequential measurement sensing steps for a large number of measurements.

III. SEQUENTIAL-BASED METROLOGY FOR LONG TRAJECTORIES

The FI is given by

$$\mathcal{F}_\lambda = \sum_\gamma P_\gamma (\partial_\lambda \ln P_\gamma)^2, \quad P_\gamma = \prod_{\gamma_i=1}^{n_{\text{seq}}} p(\gamma_i), \tag{3}$$

where $\sum_\gamma$ runs over all possible trajectories, $\partial_\lambda := \partial/\partial\lambda$, and P_γ is the conditional probability associated with a particular quantum trajectory γ. Note that the above FI quantifies the achievable precision limit for a given measurement basis, considering all trajectories γ. However, the exponential growth in the number of trajectories γ makes the computation of the FI in Eq. (3) infeasible. We now address this issue with an efficient method for arbitrary numbers of sequential measurements. To do so, let us consider the recursive formula of the FI for arbitrary n_{seq} as follows.

Proposition. The information gained about λ after performing a subsequent n measurement on the probe conditioned on all previous $n - 1$ measurements is

$$\mathcal{F}_\lambda^{(n)} = \mathcal{F}_\lambda^{(n-1)} + \Delta\mathcal{F}_\lambda^{(n)},$$
$$\Delta\mathcal{F}_\lambda^{(n)} := \sum_{\gamma^{(n-1)}} P_{\gamma^{(n-1)}} f_\lambda^{\gamma^{(n-1)}}, \tag{4}$$

where $\mathcal{F}_\lambda^{(n)}$ is the FI at step n, $\Delta\mathcal{F}_\lambda^{(n)}$ is the increment of the FI after performing one more measurement while the previous $n - 1$ outcomes have been recorded, and $f_\lambda^{\gamma^{(n-1)}}$ is the FI obtained from the nth measurement $p(\gamma_n)$ in trajectory $\gamma^{(n-1)}$, written as

$$f_\lambda^{\gamma^{(n-1)}} := \sum_{\gamma_n} \frac{\big[\partial_\lambda p(\gamma_n | \gamma^{(n-1)})\big]^2}{p(\gamma_n | \gamma^{(n-1)})}. \tag{5}$$

Proof. From conditional probabilities, one gets

$$\ln P_{\gamma^{(n)}} = \ln P_{\gamma^{(n-1)}} + \ln p(\gamma_n | \gamma^{(n-1)}), \tag{6}$$

where $\gamma^{(n)}$ is a generic trajectory with n measurement outcomes and $p(\gamma_n | \gamma^{(n-1)})$ is the conditional probability of obtaining the outcome γ_n at step n conditioned upon all $n - 1$ previous measurement outcomes. Substituting Eq. (6) into Eq. (3) (see Appendix A for details) results in

$$\mathcal{F}_\lambda^{(n)} = \mathcal{F}_\lambda^{(n-1)} + \sum_{\gamma^{(n-1)}} P_{\gamma^{(n-1)}} \sum_{\gamma_n} \frac{\big[\partial_\lambda p(\gamma_n | \gamma^{(n-1)})\big]^2}{p(\gamma_n | \gamma^{(n-1)})}, \tag{7}$$

which leads to $\mathcal{F}_\lambda^{(n)} = \mathcal{F}_\lambda^{(n-1)} + \sum_{\gamma^{(n-1)}} P_{\gamma^{(n-1)}} f_\lambda^{\gamma^{(n-1)}}$. ∎

Note that Eq. (4) is exact (i.e., no approximation or assumptions have been made). However, in order to obtain such an exact evaluation of the FI, one is required to calculate

the whole probability distributions (i.e., the whole trajectory space γ) associated with measuring the probe locally at regular time intervals. Since the whole trajectory space grows exponentially, although Eq. (4) is exact, it rapidly becomes computationally infeasible. To circumvent this issue, we employ a Monte Carlo approach to evaluate the FI for any n_{seq}, approximating the FI increment as follows:

$$\Delta \mathcal{F}_\lambda^{(n)} \sim \sum_{\mu=1}^{\mu_{\max}} \frac{f_\lambda^{\mu,(n)}}{\mu_{\max}},\tag{8}$$

where $f_\lambda^{\mu,(n)}$ is the FI obtained from $p(\gamma_n)$ in the Monte Carlo trajectory μ and $\mu_{\max}$ is the total number of Monte Carlo samplings. In the limit of $\mu_{\max} \to \infty$, Eq. (8) converges to the actual FI increment shown in Eq. (4). Note that the Monte Carlo approach automatically selects the more probable trajectories, making the simulation computationally efficient and robust even in the presence of a large number of sequential measurements n; see later discussions on numerical robustness in Sec. VI. Two key questions arise from Eq. (8): How does the increment $\Delta \mathcal{F}_\lambda^{(n)}$ of the FI behave as n increases? Is there a limit to the amount of information that can be extracted about λ as n increases? To address these issues, we shed light on two central features of sequential measurements sensing: the memory loss of the probe due to consecutive measurements and the fact that the resulting state can be well approximated by the orthonormal basis of the singular value decomposition of the combined evolution and measurement dynamics.

IV. MEMORY LOSS AND RANK-1 MATRIX

Performing n_{seq} sequential measurements on the probe's initial state ρ_0 leads to a gradual loss of information about ρ_0. To support this, consider

$$V^{(j)} := \Pi_{\gamma_j} U_\lambda^{(j)},\tag{9}$$

where $U^{(j)}$ is a unitary operator and $\Pi_{\gamma_j} = \mathbb{I} \otimes |\gamma_j\rangle\langle\gamma_j|$ is a local projection measurement. Note that in the absence of an explicit Hilbert space structure it is challenging to provide an explicit POVM Π_{γ_j}. Nonetheless, for the sake of simplicity, we have given $\Pi_{\gamma_j} = \mathbb{I} \otimes |\gamma_j\rangle\langle\gamma_j|$ only to stress that throughout this paper we consider local measurements performed on the probe. The (un-normalized) quantum state after n_{seq} steps is

$$\rho^{(n_{seq})} \sim \mathscr{P}_\lambda^{(n_{seq})} \rho_0 \mathscr{P}_\lambda^{(n_{seq})\dagger},\tag{10}$$

where

$$\mathscr{P}_\lambda^{(n_{seq})} := \prod_{j=1}^{n_{seq}} V^{(j)}.\tag{11}$$

To validate the memory loss observation, we simulate final states $\phi^{(n_{seq})}$ and $\theta^{(n_{seq})}$ resulting from two distinct random initial states $\rho_0 = \phi_0$ and $\rho_0 = \theta_0$ following the *same* quantum trajectory. We consider three $\mathscr{P}_\lambda^{(n_{seq})}$ cases.

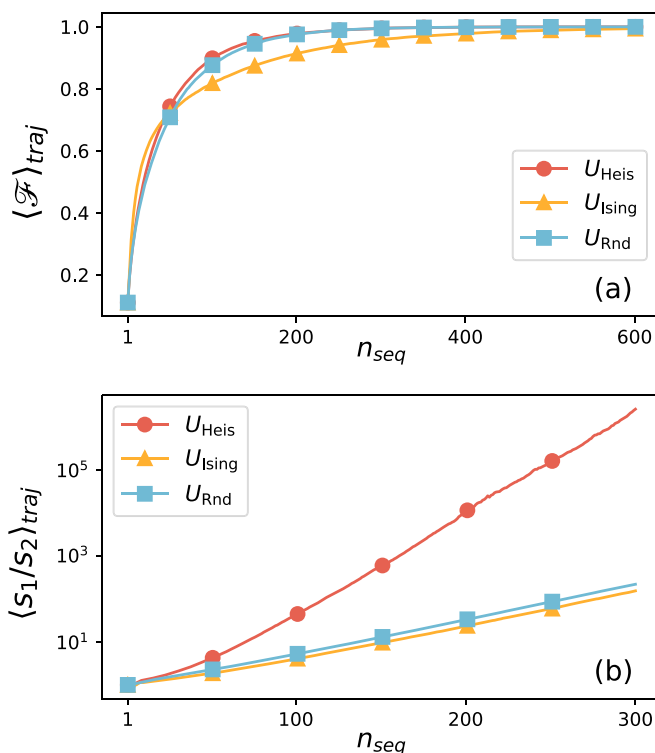(i) The first case is a random unitary U_{Rnd} measured locally in the computational basis.

FIG. 1. We compare final states $\phi^{(n_{seq})}$ and $\theta^{(n_{seq})}$ resulting from two distinct random initial states $\rho_0 = \phi_0$ and $\rho_0 = \theta_0$ following the *same* quantum trajectory. (a) Fidelity $\langle \mathscr{F} \rangle_{traj} := \langle \mathscr{F}(\phi^{(n_{seq})}, \theta^{(n_{seq})}) \rangle_{traj}$ as a function of n_{seq} for several unitary operators. (b) Ratio between the largest and second-largest singular values s_1 and s_2 as a function of n_{seq} for several unitary operators. We consider a system size of $N = 6$.

(ii) The second case is a Heisenberg unitary $U_{Heis} = \exp[-i\tau H_{Heis}]$, where

$$H_{Heis} = -J \sum_{j=1}^{N-1} \boldsymbol{\sigma}_j \cdot \boldsymbol{\sigma}_{j+1}.\tag{12}$$

(iii) The third case is an Ising unitary $U_{Ising} = \exp[-i\tau H_{Ising}]$, where

$$H_{Ising} = -J \sum_{j=1}^{N-1} \sigma_j^z \sigma_{j+1}^z + B \sum_{j=1}^{N} \sigma_j^x.\tag{13}$$

In the above, N is the system size, $\boldsymbol{\sigma}_j = (\sigma_j^x, \sigma_j^y, \sigma_j^z)$ is a vector of Pauli matrices acting at site j, $J > 0$ is the exchange interaction, and B is a magnetic field. For the Heisenberg (Ising) case we sequentially measured a single spin in the σ_z (σ_x) basis at $J\tau = N$. To quantify their distinguishability between states, we use the fidelity [69]

$$\mathscr{F} := \mathscr{F}(\phi^{(n_{seq})}, \theta^{(n_{seq})}).\tag{14}$$

In Fig. 1(a), we plot the fidelity $\langle \mathscr{F} \rangle_{traj}$ averaged over 10^4 trajectories as a function of n_{seq} for several unitary operators. As the figure shows, the fidelity goes towards unity as n_{seq} increases; namely, the resulting states are indistinguishable regardless of their initial states.

Interestingly, the total evolution-measurement operator $\mathscr{P}_\lambda^{(n_{\text{seq}})}$ approximates a rank-1 matrix as n_{seq} increases. Hence $\mathscr{P}_\lambda^{(n_{\text{seq}})}$ can be written as

$$\mathscr{P}_\lambda^{(n_{\text{seq}})} \sim |p\rangle\langle p|, \qquad (15)$$

where $|p\rangle$ is an orthonormal basis of the singular value decomposition of $\mathscr{P}_\lambda^{(n_{\text{seq}})}$. In Fig. 1(b), we plot the ratio between the largest and second-largest singular values of $\mathscr{P}_\lambda^{(n_{\text{seq}})}$, namely s_1 and s_2, as a function of n_{seq} for different unitary operators. As seen from the figure, s_1 dominates as n_{seq} increases, resulting in a rank-1 matrix in agreement with the memory loss of the initial state; see Fig. 1(a). Thus, for a given trajectory, the state of the system asymptotically approaches $|p\rangle\langle p|$ independent of its initial state, though depending on the trajectory. It is worth emphasizing that the quantum state never reaches a steady state. Indeed, at step n, it changes after a subsequent evolution followed by another measurement which extracts $f_\lambda^{\gamma^{(n)}}$ information about the unknown parameter. The resulting state belongs to a subspace of which the new state can be well approximated by an orthonormal basis of the singular value decomposition of $\mathscr{P}_\lambda^{(n+1)}$.

V. EXTRACTABLE INFORMATION LIMITS

We aim to estimate the parameter λ which is encoded in the unitary operation $U_\lambda^{(j)}$. Let us assume that $\mathscr{P}_\lambda^{(m)}$ becomes a rank-1 matrix after m sequential measurements; that is,

$$\mathscr{P}_\lambda^{(m)} \sim |p(m,\lambda)\rangle\langle p(m,\lambda)|. \qquad (16)$$

This means that for any arbitrary long sequence, the final state can always be written as

$$\rho^{(m)} \sim \mathscr{P}_\lambda^{(m)} \tilde{\rho} \mathscr{P}_\lambda^{\dagger(m)}, \qquad (17)$$

where $\tilde{\rho}$ is any density matrix independent of λ. Since m is a finite number of sequential steps, the FI that can be accumulated throughout this process can only be finite. The above statement implies

$$\Delta\mathcal{F}_\lambda^{(j)} = \sum_{\gamma^{(j-1)}} P_{\gamma^{(j-1)}} f_\lambda^{\gamma^{(j-1)}} \leqslant f_\lambda^{\max} \sim G\big(\mathscr{P}_\lambda^{(m)}\big), \qquad (18)$$

where $f_\lambda^{\max} = \max_{\gamma^{(n-1)}}[f_\lambda^{\gamma^{(n-1)}}]$ and $G(\mathscr{P}_\lambda^{(m)})$ is a finite function depending on $\mathscr{P}_\lambda^{(m)}$. Hence, at each measurement step, one can, at best, add $G(\mathscr{P}_\lambda^{(m)})$ to the FI. The direct consequence is that the FI is bounded by a linear function of the number of sequential measurements m. In the following, we provide three distinct physical systems to support our findings.

A. Example 1: Spin chain magnetometry

We consider N spin-1/2 particles with Heisenberg interaction in the presence of a local magnetic field B, which we aim to estimate with sequential metrology. The Hamiltonian is

$$H = -J \sum_{j=1}^{N-1} \boldsymbol{\sigma}_j \cdot \boldsymbol{\sigma}_{j+1} + B\sigma_1^x, \qquad (19)$$

where $J > 0$ is the exchange interaction and B is a magnetic field. Without loss of generality, we consider a probe size
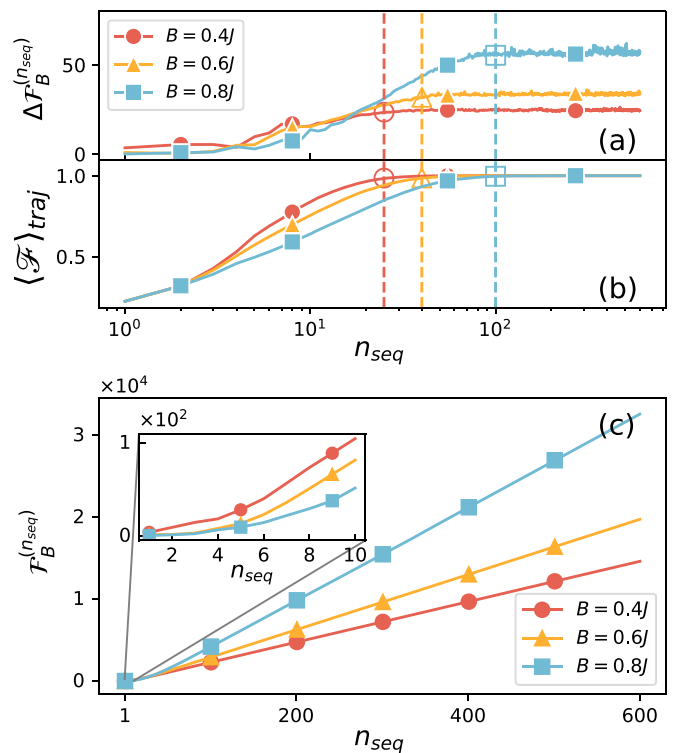

FIG. 2. (a) FI increment $\Delta\mathcal{F}_B^{(n_{\text{seq}})}$ as a function of n_{seq} for various B. (b) Averaged fidelity $\langle\mathscr{F}\rangle_{\text{traj}}$ as a function of n_{seq} for various B. Dashed lines divide the curves into a nontrivial (memory) and constant (memoryless) dependence on n_{seq}. (c) $\mathcal{F}_B^{(n_{\text{seq}})}$ as a function of n_{seq} for several values of B.

$N = 4$, where each trajectory initializes in $|\psi(0)\rangle = |\downarrow\rangle^{\otimes N}$, evolves unitarily at regular times $J\tau_i = J\tau = N$ under $U^{(j)} = U = e^{-i\tau H}$, and is measured sequentially at local site N in the σ_z basis. In Fig. 2(a), we plot the FI increment $\Delta\mathcal{F}_B^{(n_{\text{seq}})}$ averaged over 10^5 trajectories [see Eq. (8)] as a function of n_{seq} for several values of B. As the figure shows, $\Delta\mathcal{F}_B^{(n_{\text{seq}})}$ initially grows with increasing n_{seq} and then saturates to an approximately constant value. The transition has been specified by a dashed line. To link the memory loss feature with the above nontrivial behavior of $\Delta\mathcal{F}_B^{(n_{\text{seq}})}$, we simulate final states $\phi^{(n_{\text{seq}})}$ and $\theta^{(n_{\text{seq}})}$ resulting from two distinct random initial states $\rho_0 = \phi_0$ and $\rho_0 = \theta_0$ following the *same* quantum trajectory. In Fig. 2(b), we plot the fidelity $\langle\mathscr{F}\rangle_{\text{traj}}$ averaged over 10^4 trajectories as a function of n_{seq} for several values of B. Remarkably, as seen from the figure, a clear correspondence between the nontrivial dependence of $\Delta\mathcal{F}_B^{(n_{\text{seq}})}$ with respect to n_{seq} and the loss of memory with respect to the probe's initial state emerges; see dashed lines in Figs. 2(a) and 2(b). Indeed, as the probe keeps the memory of the initial state, the FI increment grows nonlinearly with respect to n_{seq}. Conversely, when the probe loses its memory of the initial state, the FI increment reaches an approximate constant value. Thus the FI can only grow linearly with n_{seq}. This is explicitly depicted in Fig. 2(c), where we plot the FI $\mathcal{F}_B^{(n_{\text{seq}})}$ as a function of n_{seq} for several values of B. As shown in the figure, a clear superlinear behavior (inset) transits to a linear behavior as n_{seq} increases.

B. Example 2: Light-matter interaction

We consider the Jaynes-Cummings (JC) model which describes the interaction between a two-level atom and a quantized radiation field [70]. The Hamiltonian is

$$H_{\text{JC}} = \hbar\omega_c a^\dagger a + \tfrac{1}{2}\hbar\omega_a \sigma^z + \hbar\Omega(\sigma^+ a + \sigma^- a^\dagger), \qquad (20)$$

where a ($a^\dagger$) is the annihilation (creation) operator; $\sigma^z = |e\rangle\langle e| - |g\rangle\langle g|$, $\sigma^+ = |e\rangle\langle g|$, and $\sigma^- = |g\rangle\langle e|$, where $|g\rangle$ ($|e\rangle$) is the ground (excited) state of the two-level atom; ω_c is the frequency of the field; ω_a is the two-level atom's transition frequency; and Ω is the atom-field coupling strength. We aim to estimate Ω using sequential measurements on the atom. Without loss of generality, $\omega_c = \omega_a = \omega$, we initialize each trajectory from $|\psi(0)\rangle = |g\rangle|\alpha\rangle$, where $|\alpha\rangle$ is a coherent state, and measurements are performed at $\omega\tau = 2\pi$ intervals. Notably, for $n_{\text{seq}} \gg 1$, the field will likely be filtered into a specific number state $|\tilde{m}\rangle$ (see Appendix B for details). This implies that the atom-field state evolves within the subspace $\{|e, \tilde{m}\rangle, |g, \tilde{m}+1\rangle\}$, with $\Delta\mathcal{F}_\Omega^{(n_{\text{seq}})} \sim \tau^2(\tilde{m}+1)$. Hence, for a fixed evolution time τ and number state $\tilde{m}$, the FI increment is bounded in agreement with Eq. (18). In Fig. 3(a), we plot the FI increment $\Delta\mathcal{F}_\Omega^{(n_{\text{seq}})}$ as a function of n_{seq} for two coupling strengths Ω. As the figure shows, the transition between non-trivial behavior and a constant value of $\Delta\mathcal{F}_\Omega^{(n_{\text{seq}})}$ concerning n_{seq} holds. Thus the FI can only grow linearly with extra measurements. In Fig. 3(b), we plot the FI $\mathcal{F}_\Omega^{(n_{\text{seq}})}$ as a function of n_{seq} for two values of Ω. The figure shows a clear transition from nonlinear to linear behavior.

C. Example 3: Nonunitary dynamics

To demonstrate the generality of our analysis, we show that our results still hold for nonunitary dynamics. We consider the spin chain of Eq. (19) with $B = 0$,

$$H = -J \sum_{j=1}^{N-1} \boldsymbol{\sigma}_j \cdot \boldsymbol{\sigma}_{j+1}, \qquad (21)$$

subjected to local dissipation:

$$\dot{\rho} = -\frac{i}{\hbar}[H, \rho] + \kappa \sum_{i=1}^{N}[(1+n_{\text{th}})\mathcal{D}[\sigma_i^-]\rho + n_{\text{th}}\mathcal{D}[\sigma_i^+]\rho], \qquad (22)$$

where $\mathcal{D}[O]\rho = O\rho O^\dagger - \frac{1}{2}\{O^\dagger O, \rho\}$, $\{\cdot, \cdot\}$ is the anticommutator, κ is the decay rate, and n_{th} is the average number of bath excitations. We aim to estimate κ using local sequential measurements on the spin at site N. In Fig. 3(c), we plot the FI increment $\Delta\mathcal{F}_\kappa^{(n_{\text{seq}})}$ as a function of n_{seq} for two values of κ. As seen from the figure, a clear constant saturation of $\Delta\mathcal{F}_\kappa^{(n_{\text{seq}})}$ is reached for both cases, demonstrating that a finite amount of information can be extracted at each step even for nonunitary dynamics. In Fig. 3(d), we plot the FI $\mathcal{F}_\kappa^{(n_{\text{seq}})}$ as a function of n_{seq} for two values of κ. The figure demonstrates an evident transition from nonlinear to linear behavior.
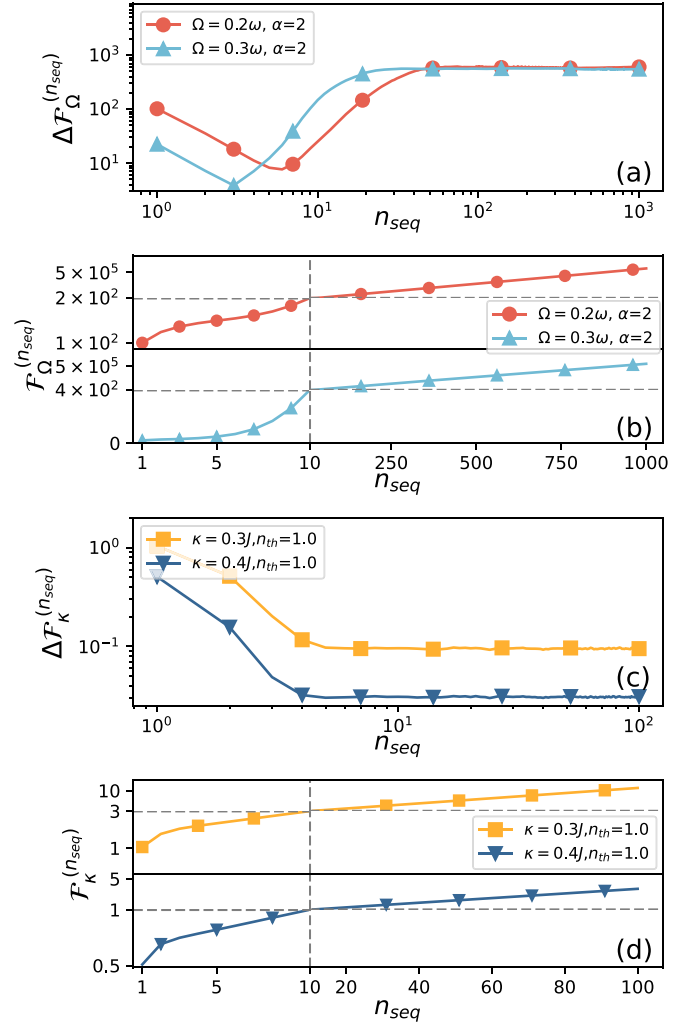

FIG. 3. JC model case: (a) $\Delta\mathcal{F}_\Omega^{(n_{\text{seq}})}$ as a function of n_{seq} for various Ω; (b) $\mathcal{F}_\Omega^{(n_{\text{seq}})}$ as a function of n_{seq} for several Ω. Nonunitary case: (c) $\Delta\mathcal{F}_\kappa^{(n_{\text{seq}})}$ as a function of n_{seq} for different values of κ; (d) $\mathcal{F}_\kappa^{(n_{\text{seq}})}$ as a function of n_{seq} for various κ.

VI. ROBUSTNESS ANALYSIS

This section demonstrates the high accuracy of our numerical simulations using the Monte Carlo approximation method for calculating the FI, specifically its FI increment shown in Eq. (8). Throughout this section, we use the following notation: The FI approximated using the Monte Carlo approach is denoted as $\mathcal{F}^{\text{MC}}$, and the FI computed from exact probability distributions is denoted as $\mathcal{F}^{\text{exact}}$. Moreover, we analyze the numerical robustness for the three examples considered above, namely spin chain magnetometry, light-matter (Jaynes-Cummings) interaction, and nonunitary dynamics.

We first focus our analysis on comparing the relative error between $\mathcal{F}^{\text{MC}}$ and $\mathcal{F}^{\text{exact}}$ as the number of Monte Carlo trajectories grows [μ_{max} in Eq. (8)]. To do so, we consider the relative error between these quantities as

$$\text{relative error}\big(\mathcal{F}_i^{\text{MC}}, \mathcal{F}_i^{\text{exact}}\big) = \frac{\big|\mathcal{F}_i^{\text{MC}} - \mathcal{F}_i^{\text{exact}}\big|}{\mathcal{F}_i^{\text{exact}}}, \qquad (23)$$
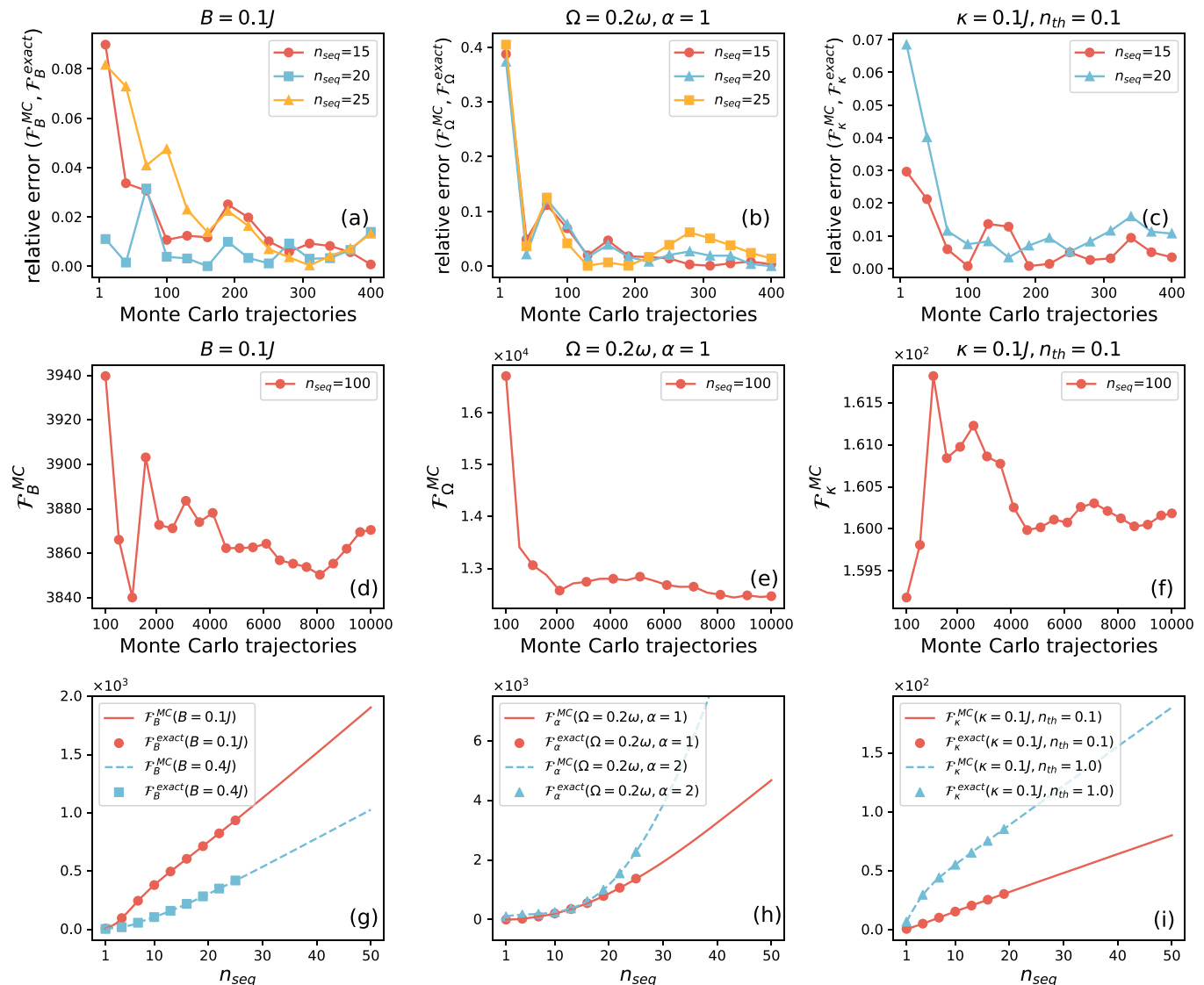
FIG. 4. Relative error between the Monte Carlo FI $\mathcal{F}^{MC}$ and the exact FI $\mathcal{F}^{exact}$ as a function of the number of Monte Carlo trajectories for the (a) spin chain, (b) light-matter interaction, and (c) nonunitary dynamics examples. The relative error decreases to around 1% as the number of trajectories increases for all three cases. Monte Carlo FI $\mathcal{F}^{MC}$ as a function of the number of Monte Carlo trajectories for a fixed sequential measurement number $n_{seq} = 100$, for the (d) spin chain, (e) light-matter interaction, and (f) nonunitary dynamics cases. A clear convergence of $\mathcal{F}^{MC}$ towards a stationary value emerges as the number of Monte Carlo trajectories increases. Exact FI and Monte Carlo FI as a function of the number of sequential measurements n_{seq} for various parameter values, for the (g) spin chain, (h) light-matter interaction, and (i) nonunitary dynamics scenarios. The curves closely overlap, demonstrating the accuracy of our procedure.

where i refers to B, Ω, and κ for the spin chain, light-matter, and nonunitary examples, respectively.

In Figs. 4(a)–4(c), we plot the relative error between $\mathcal{F}^{MC}$ and $\mathcal{F}^{exact}$ as a function of the number of Monte Carlo trajectories. As the figures show, there is a prompt reduction of the relative error for all three cases. Particularly, for this specific set of parameters, the number of trajectories needed to go below 1% is of the order of 10^2. It is worth noting that throughout our numerical simulations in this paper, we typically used from 10^4 to 10^5 trajectories to ensure high accuracy as other system parameters increase, e.g., when n_{seq} is of the order of 10^2. In general, our numerical simulations are robust as the relative error reduces across all scenarios. To further support the robustness analysis, in Figs. 4(d)–4(f) we plot $\mathcal{F}^{MC}$ as a function of the Monte Carlo trajectories for a fixed number of se-

quential measurements $n_{seq} = 100$. As seen from the figures, the FI approximated via the Monte Carlo approach quickly converges to a stationary value across all examples. Finally, in Figs. 4(g)–4(i), we plot $\mathcal{F}^{MC}$ and $\mathcal{F}^{exact}$ individually as a function of n_{seq}. It is worth noting that for the exact case, we are able to simulate up to ~30 sequential measurements, as higher values are extremely computationally costly. However, for the area in which both can be compared, the results almost overlap. Therefore our methodology stands as a reliable one with very small relative error and quick convergence.

VII. RESOURCE ANALYSIS

Any sensing protocol requires that the available sensing resources such as time or number of particles be defined.
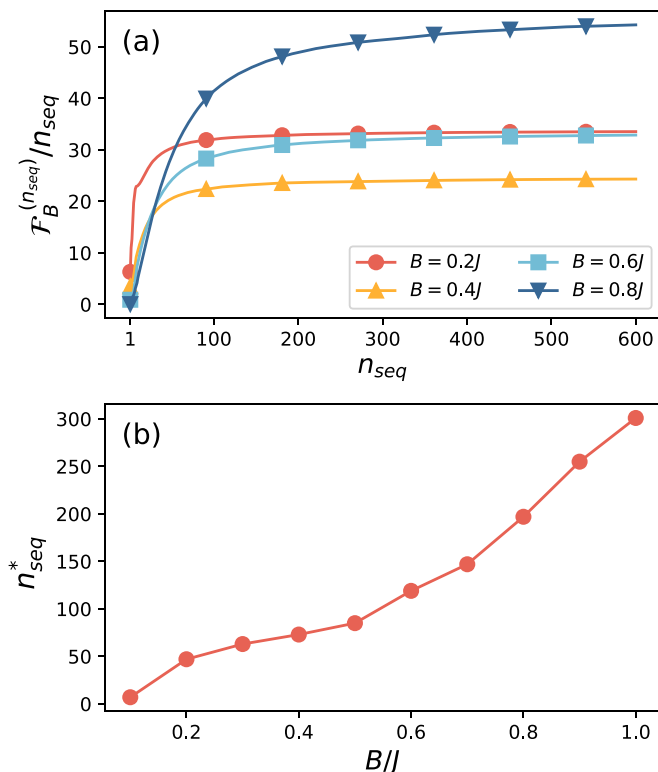
FIG. 5. (a) Gain $\mathcal{F}_B^{(n_{\text{seq}})}/n_{\text{seq}}$ as a function of n_{seq} for different values of B. (b) n_{seq}^* as a function of B.

Therefore the sensing benefits in relation to these resources must be determined. In what follows, we consider two scenarios relevant to experimental realizations using sequential measurements sensing schemes: the number of total measurements performed on the probe and the total sensing protocol time.

A. Measurements as resource

When should we reset the sensing protocol to maximize the potential of the sequential measurement scheme? To address this issue, we consider the total number of measurements, $Mn_{\text{seq}} = R$, as our sensing resource R. This constraint causes the Cramér-Rao inequality to be

$$\text{Var}[\lambda] \geqslant \frac{1}{R\frac{\mathcal{F}_\lambda^{(n_{\text{seq}})}}{n_{\text{seq}}}}, \tag{24}$$

where $\text{Var}[\lambda]$ is the variance of λ. Clearly, the *gain* $\mathcal{F}_\lambda^{(n_{\text{seq}})}/n_{\text{seq}}$ determines the step n_{seq} to cease the protocol and initiate a new trajectory. The larger the gain, the smaller the uncertainty provided by the sequential measurement protocol. Based on the first example, in Fig. 5(a), we plot the gain $\mathcal{F}_B^{(n_{\text{seq}})}/n_{\text{seq}}$ as a function of n_{seq} for different B. As the figure shows, the gain slows down after a specific n_{seq} for all B. This suggests that after a certain n_{seq} the protocol provides marginal benefits. We denote n_{seq}^* as the n_{seq} such that $\mathcal{F}_B^{(n_{\text{seq}}^*)}/n_{\text{seq}}^*$ is over 90% of the saturated value at $n_{\text{seq}} = 600$. In Fig. 5(b), we plot n_{seq}^* as a function of B. As the figure shows, n_{seq}^* grows monotonically

as B increases. This means that for larger B one should stop the sensing protocol after longer sequential measurements.

B. Time as resource

Thus far, we have considered the total number of measurements as our main sensing resource. With this approach, we were able to determine the specific n_{seq}^* at which we needed to stop a particular trajectory and start a newly fresh trajectory. This allowed us to exploit the sequential measurements scheme optimally with respect to that sensing resource. Nonetheless, time can also be accounted for as a sensing resource. To consider time as a resource, we follow Ref. [67], where the total protocol time T is defined as

$$T = M(t_{\text{reset}} + n_{\text{seq}}t_{\text{meas}} + n_{\text{seq}}\tau), \tag{25}$$

where M is the total number of trajectories, t_{reset} is the time it takes to reset each trajectory, t_{meas} is the time it takes to measure the particle, τ is the free-evolution time between measurements, and n_{seq} is the number of sequential measurements. It is typical in experiments that the resetting time is larger than the time it takes to measure a subsystem. Thus we consider $t_{\text{meas}} = 10\tau$, while t_{reset} is found to be in the range $0 \leqslant t_{\text{reset}} \leqslant 4000\tau$.

By recalling the Cramér-Rao inequality, one obtains that the variance of the unknown parameter relates to the inverse of the FI, i.e., $\text{Var}[\lambda] \geqslant (\mathcal{F})^{-1}$. Therefore the lower the FI inverse, the lower the uncertainty.

Having this relationship at hand, in Figs. 6(a)–6(c) we plot the inverse FI (approximated using the Monte Carlo approach) as a function of n_{seq} for several values of t_{reset} for a fixed total protocol time T. As seen from the figures, all cases show that the best scenario is the *ideal* case where $t_{\text{reset}} = 0$. However, once $t_{\text{reset}} \neq 0$, the results show that one can truly benefit from consecutively measuring the system. Interestingly, Figs. 6(a)–6(c) all show that for the same fixed total protocol time T, a very long number of sequential measurements proves to be very beneficial for reducing the uncertainty of the unknown parameter. In other words, since resetting the system is very costly, one could spend the entire time measuring the system constrained to the same total protocol time T, achieving similar sensing performance with a very large number of sequential measurements.

VIII. CONCLUSIONS

We introduce a recursive formula and an efficient Monte Carlo approach to evaluate the Fisher information for sequential measurements sensing of arbitrary lengths. Our findings show that the obtainable Fisher information initially grows nonlinearly with respect to the number of measurements and then asymptotically saturates to a linear function. This transition is directly linked to the probe's finite memory of an early state. When the memory of such early state is lost, the information accumulation about the unknown parameter (i.e., incremental FI) becomes almost constant, resulting in linear scaling of the FI. This fundamentally limits the extractable information capacity through sequential measurements. Finally, we considered the total number of measurements and the total protocol time as main sensing resources and
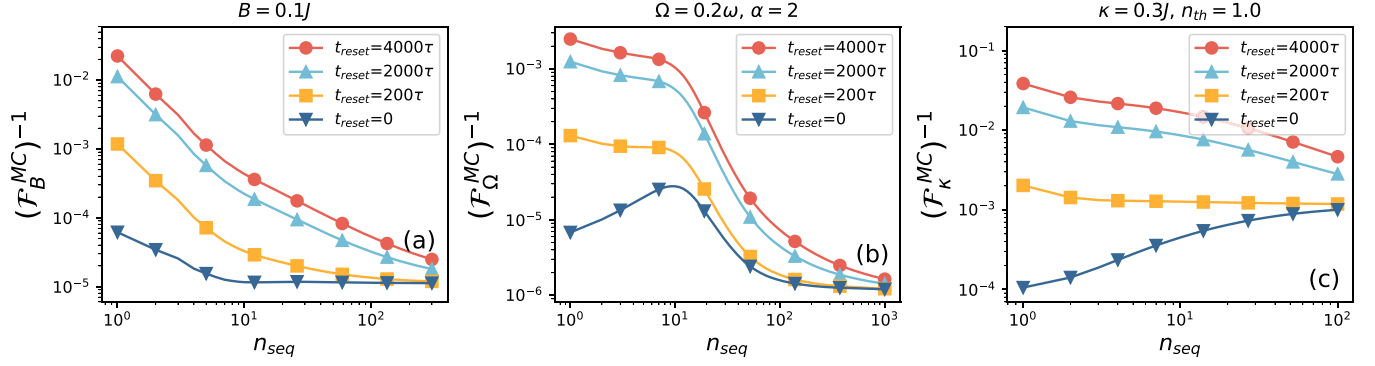
FIG. 6. Inverse of the Monte Carlo FI $\mathcal{F}^{\mathrm{MC}}$ as a function of n_{seq} for several resetting times t_{reset}: (a) spin chain case, (b) Jaynes-Cummings case, and (c) nonunitary dynamics case. We consider the measurement time as $t_{\mathrm{meas}} = 10\tau$, where τ is the free-evolution time between measurements. In particular, we chose $J\tau = 4$ for the spin chain case, $\omega\tau = 2\pi$ for the Jaynes-Cummings case, and $J\tau = 1$ for the nonunitary case, respectively. Other parameters are shown in the figure.

established a figure of merit to identify the optimal measurement sequence length. Establishing such a resetting point is relevant in practice due to the limited coherence time of the probe and the limited number of sequential measurements that can be performed. We exemplified our results in three distinct physical systems.

Our study bridges the gap between several previous studies connecting the initial superlinear growth of the Fisher information [67] to the linear scaling at a large number of measurement sequences, which previously could be addressed only through indirect methods [56,68]. Although our protocol assumes minimal control, it can be improved by employing quantum control for updating measurements at each sequence or mitigating possible noise in practical scenarios [71].

APPENDIX A: PROOF OF THE RECURSIVE FORMULA FOR FISHER INFORMATION IN SEQUENTIAL MEASUREMENTS METROLOGY

The following proof follows Ref. [41]. Here, we reformulate it to fit our sequential measurements sensing protocol. The Fisher information (FI) takes into account all (n) sequential measurement outcomes, $\gamma^{(n)} = (\gamma_1, \gamma_2, \ldots, \gamma_n)$, and can be expressed as follows:

$$\mathcal{F}_{\lambda}^{(n)} = E_{\gamma^{(n)}}\left[\left(\frac{\partial \ln P_{\gamma^{(n)}}(\lambda)}{\partial \lambda}\right)^2\right], \quad (\mathrm{A1})$$

where $E[\cdot]$ is the expectation value of "$\cdot$" (here, with a countable set of possible outcomes) and $P_{\gamma^{(n)}}$ denotes the

conditional probability of the random variable $\gamma^{(n)}$ for n consecutive outcomes.

According to the definition in Eq. (3) (see main text), the probability associated with a specific trajectory exhibits the following simple relationship:

$$\ln P_{\gamma^{(n)}}(\lambda) = \ln P_{\gamma^{(n-1)}}(\lambda) + \ln p(\gamma_n \mid \gamma^{(n-1)}; \lambda), \quad (\mathrm{A2})$$

where $p(\gamma_n \mid \gamma^{(n-1)}; \lambda)$ accounts for the conditional probability of obtaining γ_n as the outcome of the nth sequential measurement conditioned on $(n-1)$ previous measurements, i.e., conditioned on the trajectory $\gamma^{(n-1)}$.

By substituting Eq. (A2) into Eq. (A1), one obtains

$$\mathcal{F}^{(n)} = E_{\gamma^{(n)}}\left[\left(\frac{\partial \ln P_{\gamma^{(n-1)}}(\lambda)}{\partial \lambda}\right)^2\right]$$

$$+ E_{\gamma^{(n)}}\left[\left(\frac{\partial \ln p(\gamma_n \mid \gamma^{(n-1)}; \lambda)}{\partial \lambda}\right)^2\right]$$

$$+ 2 \cdot E_{\gamma^{(n)}}\left[\left(\frac{\partial \ln P_{\gamma^{(n-1)}}(\lambda)}{\partial \lambda}\right)\left(\frac{\partial \ln p(\gamma_n \mid \gamma^{(n-1)}; \lambda)}{\partial \lambda}\right)\right], \quad (\mathrm{A3})$$

where the first term on the right-hand side of Eq. (A3) can be written as $E_{\gamma^{(n)}}[(\frac{\partial \ln P_{\gamma^{(n-1)}}(\lambda)}{\partial \lambda})^2] =: \mathcal{F}^{(n-1)}$. The last cross term on the right-hand side of Eq. (A3) can be expressed as follows:

$$E_{\gamma^{(n)}}\left[\left(\frac{\partial \ln P_{\gamma^{(n-1)}}(\lambda)}{\partial \lambda}\right)\left(\frac{\partial \ln p(\gamma_n \mid \gamma^{(n-1)}; \lambda)}{\partial \lambda}\right)\right]$$

$$= \sum_{\gamma^{(n)}} P_{\gamma^{(n)}}(\lambda)\left(\frac{\partial \ln P_{\gamma^{(n-1)}}(\lambda)}{\partial \lambda} \cdot \frac{\partial \ln p(\gamma_n \mid \gamma^{(n-1)}; \lambda)}{\partial \lambda}\right)$$

$$= \sum_{\gamma^{(n-1)}} P_{\gamma^{(n-1)}}(\lambda)\left(\frac{\partial \ln P_{\gamma^{(n-1)}}(\lambda)}{\partial \lambda}\right)$$

$$\times \sum_{\gamma_n} p(\gamma_n \mid \gamma^{(n-1)}; \lambda)\left(\frac{\partial \ln p(\gamma_n \mid \gamma^{(n-1)}; \lambda)}{\partial \lambda}\right). \quad (\mathrm{A4})$$
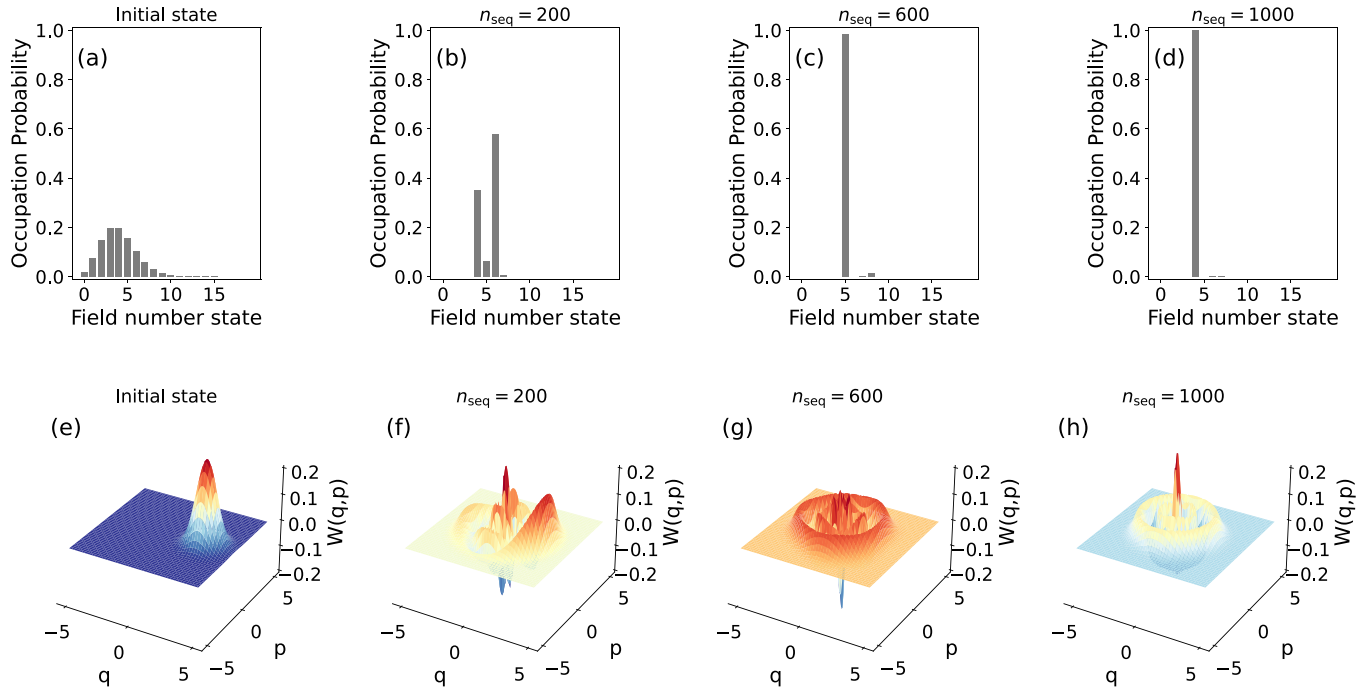
FIG. 7. (a)–(d) The occupation probability of the field as a function of its number state for different n_{seq}. (e)–(h) The Wigner function for the field state for different n_{seq} instances. This figure demonstrates that the field, under Jaynes-Cummings interaction, is likely to collapse into a single number state after the qubit is measured repeatedly.

Note that

$$\sum_{\gamma_n} p\big(\gamma_n \mid \gamma^{(n-1)}; \lambda\big)\left(\frac{\partial \ln p(\gamma_n \mid \gamma^{(n-1)}; \lambda)}{\partial \lambda}\right)$$

$$= \partial_\lambda \sum_{\gamma_n} p\big(\gamma_n \mid \gamma^{(n-1)}; \lambda\big) = 0, \qquad \text{(A5)}$$

and therefore the cross term vanishes. Equation (A3) simply reduces to

$$\mathcal{F}^{(n)} = \mathcal{F}^{(n-1)} + E_{\gamma^{(n)}}\left[\left(\frac{\partial \ln p(\gamma_n \mid \gamma^{(n-1)}; \lambda)}{\partial \lambda}\right)^2\right]. \quad \text{(A6)}$$

By expanding the second term on the right-hand side of Eq. (A6), one gets

$$E_{\gamma^{(n)}}\left[\left(\frac{\partial \ln p(\gamma_n \mid \gamma^{(n-1)}; \lambda)}{\partial \lambda}\right)^2\right]$$

$$= \sum_{\gamma^{(n-1)}} P_{\gamma^{(n-1)}} E_{\gamma_n}\left[\left(\frac{\partial \ln p(\gamma_n \mid \gamma^{(n-1)}; \lambda)}{\partial \lambda}\right)^2\right]$$

$$= \sum_{\gamma^{(n-1)}} P_{\gamma^{(n-1)}} \sum_{\gamma_n} \frac{\big[\partial_\lambda p(\gamma_n|\gamma^{(n-1)})\big]^2}{p(\gamma_n|\gamma^{(n-1)})}$$

$$= \sum_{\gamma^{(n-1)}} P_{\gamma^{(n-1)}} f_\lambda^{\gamma^{(n-1)}}, \qquad \text{(A7)}$$

where we have defined $f_\lambda^{\gamma^{(n-1)}}$ as the FI obtained from the nth measurement probability distribution $p(\gamma_n \mid \gamma^{(n-1)}; \lambda)$ in the trajectory $\gamma^{(n-1)}$. Therefore the recursive formula for the FI in

the sequential measurement metrology reads as

$$\mathcal{F}_\lambda^{(n)} = \mathcal{F}_\lambda^{(n-1)} + \sum_{\gamma^{(n-1)}} P_{\gamma^{(n-1)}} f_\lambda^{\gamma^{(n-1)}}. \qquad \text{(A8)}$$

APPENDIX B: JAYNES-CUMMINGS FILTERING TOWARDS A FOCK NUMBER STATE

For the Jaynes-Cummings example, we stated that after many sequential steps, the cavity field is likely to collapse into a single number state, denoted $|\tilde{m}\rangle$ in the main text. Here, we present numerical evidence to support such a statement.

Let us start from the Jaynes-Cummings Hamiltonian H_{JC} [see Eq. (20) in the main text for details on the notation]:

$$H_{\text{JC}} = \hbar\omega a^\dagger a + \tfrac{1}{2}\hbar\omega\sigma^z + \hbar\Omega(\sigma^+ a + \sigma^- a^\dagger). \qquad \text{(B1)}$$

By initializing each trajectory from $|\psi(0)\rangle = |g\rangle|\alpha\rangle$, where $|\alpha\rangle = \sum_m \mathcal{C}(m)|m\rangle$ is a coherent state of amplitude α, here $\alpha \in \mathbb{R}e$, and

$$\mathcal{C}(m) = e^{-\frac{\alpha^2}{2}} \frac{\alpha^m}{\sqrt{m!}}, \qquad \text{(B2)}$$

one obtains the evolved wave function as

$$|\psi(t)\rangle = e^{-i\omega t H_{\text{JC}}} |\psi(0)\rangle$$

$$= \sum_m \mathcal{C}_g(m)|g, m\rangle + \mathcal{C}_e(m)|e, m-1\rangle, \qquad \text{(B3)}$$

where the field distributions associated with the states $|g\rangle$ and $|e\rangle$ are

$$\mathcal{C}_g(m) = \mathcal{C}(m)e^{-im\omega t} \cos(\sqrt{m}\Omega t), \qquad \text{(B4)}$$

$$\mathcal{C}_e(m) = -i\mathcal{C}(m)e^{-im\omega t} \sin(\sqrt{m}\Omega t). \qquad \text{(B5)}$$

Note that the initial probability field distribution, namely $\mathcal{P}_0(n) = |\mathcal{C}(n)|^2$, is now *split* into $\mathcal{P}_g(n) = |\mathcal{C}_g(n)|^2$ and $\mathcal{P}_e(n) = |\mathcal{C}e(n)|^2$. This is the core of the filtering process. By performing local measurements n_{seq} times on the qubit sequentially, here at (scaled) times 2π, the number state distribution filters to new distributions associated with states $|g\rangle$ or $|e\rangle$.

In Fig. 7 we present the sequential measurements procedure for a representative trajectory. Figures 7(a)–7(d) show the field probability occupation as a function of the field number. As the figures show, the initial coherent distribution in Fig. 7(a) is subsequently filtered as the value of n_{seq} increases, collapsing ultimately into a single field state $|\tilde{m}\rangle$ as seen in Fig. 7(d). Note that this represents a trajectory that is likely to happen; however, other field distributions can indeed occur. This is because the distributions accompanying the qubit states $\mathcal{C}_g(m)$ and $\mathcal{C}_e(m)$ (see above discussion) depend on Ω, the number state m, and the measurement time t as well. Therefore the filtering is conditioned upon other system parameters. Unwanted collapsing states can further be filtered by properly tuning the above. To further discuss the filtering case, we consider the Wigner quasiprobability distribution of the field to observe its behavior in phase space. The Wigner quasiprobability distribution is defined as follows:

$$W(q, p) = \frac{1}{\pi \hbar} \int_{-\infty}^{\infty} \langle q - y | \rho_{\text{field}} | q + y \rangle e^{2ipy/\hbar} dy. \quad \text{(B6)}$$

In Figs. 7(e)–7(h), we show the Wigner function $W(q, p)$ for different n_{seq}, namely collapsed instances of the field state. As the figures show, the initial field distribution shown in Fig. 7(e), $W(q, p) > 0$, becomes more and more narrow as n_{seq} increases, with Fig. 7(h) showing a clear single field number state $|\tilde{m}\rangle = 4$.

[1] C. L. Degen, F. Reinhard, and P. Cappellaro, Quantum sensing, Rev. Mod. Phys. **89**, 035002 (2017).

[2] A. N. Boto, P. Kok, D. S. Abrams, S. L. Braunstein, C. P. Williams, and J. P. Dowling, Quantum interferometric optical lithography: Exploiting entanglement to beat the diffraction limit, Phys. Rev. Lett. **85**, 2733 (2000).

[3] D. Leibfried, M. D. Barrett, T. Schaetz, J. Britton, J. Chiaverini, W. M. Itano, J. D. Jost, C. Langer, and D. J. Wineland, Toward Heisenberg-limited spectroscopy with multiparticle entangled states, Science **304**, 1476 (2004).

[4] V. Giovannetti, S. Lloyd, and L. Maccone, Quantum-enhanced measurements: Beating the standard quantum limit, Science **306**, 1330 (2004).

[5] V. Giovannetti, S. Lloyd, and L. Maccone, Quantum metrology, Phys. Rev. Lett. **96**, 010401 (2006).

[6] V. Giovannetti, S. Lloyd, and L. Maccone, Advances in quantum metrology, Nat. Photonics **5**, 222 (2011).

[7] F. Fröwis and W. Dür, Stable macroscopic quantum superpositions, Phys. Rev. Lett. **106**, 110402 (2011).

[8] R. Demkowicz-Dobrzański, J. Kołodyński, and M. Guţă, The elusive Heisenberg limit in quantum-enhanced metrology, Nat. Commun. **3**, 1063 (2012).

[9] D.-S. Ding, Z.-K. Liu, B.-S. Shi, G.-C. Guo, K. Mølmer, and C. S. Adams, Enhanced metrology at the critical point of a many-body Rydberg atomic system, Nat. Phys. **18**, 1447 (2022).

[10] R. Liu, Y. Chen, M. Jiang, X. Yang, Z. Wu, Y. Li, H. Yuan, X. Peng, and J. Du, Experimental critical quantum metrology with the Heisenberg scaling, npj Quantum Inf. **7**, 170 (2021).

[11] P. Zanardi, M. G. A. Paris, and L. Campos Venuti, Quantum criticality as a resource for quantum estimation, Phys. Rev. A **78**, 042105 (2008).

[12] C. Invernizzi, M. Korbman, L. C. Venuti, and M. G. A. Paris, Optimal quantum estimation in spin systems at criticality, Phys. Rev. A **78**, 042106 (2008).

[13] G. Salvatori, A. Mandarino, and M. G. A. Paris, Quantum metrology in Lipkin-Meshkov-Glick critical systems, Phys. Rev. A **90**, 022111 (2014).

[14] P. Zanardi, H. T. Quan, X. Wang, and C. P. Sun, Mixed-state fidelity and quantum criticality at finite temperature, Phys. Rev. A **75**, 032109 (2007).

[15] L. Garbe, M. Bina, A. Keller, M. G. A. Paris, and S. Felicetti, Critical quantum metrology with a finite-component quantum phase transition, Phys. Rev. Lett. **124**, 120504 (2020).

[16] Y. Chu, S. Zhang, B. Yu, and J. Cai, Dynamic framework for criticality-enhanced quantum sensing, Phys. Rev. Lett. **126**, 010502 (2021).

[17] M. M. Rams, P. Sierant, O. Dutta, P. Horodecki, and J. Zakrzewski, At the limits of criticality-based quantum metrology: Apparent super-Heisenberg scaling revisited, Phys. Rev. X **8**, 021022 (2018).

[18] S. Sarkar, C. Mukhopadhyay, A. Alase, and A. Bayat, Free-fermionic topological quantum sensors, Phys. Rev. Lett. **129**, 090503 (2022).

[19] V. Montenegro, U. Mishra, and A. Bayat, Global sensing and its impact for quantum many-body probes with criticality, Phys. Rev. Lett. **126**, 200501 (2021).

[20] J. J. Meyer, J. Borregaard, and J. Eisert, A variational toolbox for quantum multi-parameter estimation, npj Quantum Inf. **7**, 89 (2021).

[21] C. D. Marciniak, T. Feldker, I. Pogorelov, R. Kaubruegger, D. V. Vasilyev, R. van Bijnen, P. Schindler, P. Zoller, R. Blatt, and T. Monz, Optimal metrology with programmable quantum sensors, Nature (London) **603**, 604 (2022).

[22] J. Yang, S. Pang, Z. Chen, A. N. Jordan, and A. del Campo, Variational principle for optimal quantum controls in quantum metrology, Phys. Rev. Lett. **128**, 160505 (2022).

[23] B. L. Higgins, D. W. Berry, S. D. Bartlett, H. M. Wiseman, and G. J. Pryde, Entanglement-free Heisenberg-limited phase estimation, Nature (London) **450**, 393 (2007).

[24] R. S. Said, D. W. Berry, and J. Twamley, Nanoscale magnetometry using a single-spin system in diamond, Phys. Rev. B **83**, 125410 (2011).

[25] D. W. Berry, B. L. Higgins, S. D. Bartlett, M. W. Mitchell, G. J. Pryde, and H. M. Wiseman, How to perform the most accurate possible phase measurements, Phys. Rev. A **80**, 052114 (2009).

[26] B. L. Higgins, D. W. Berry, S. D. Bartlett, M. W. Mitchell, H. M. Wiseman, and G. J. Pryde, Demonstrating Heisenberg-limited unambiguous phase estimation without adaptive measurements, New J. Phys. **11**, 073023 (2009).

[27] C. Bonato, M. S. Blok, H. T. Dinani, D. W. Berry, M. L. Markham, D. J. Twitchen, and R. Hanson, Optimized quantum sensing with a single electron spin using real-time adaptive measurements, Nat. Nanotechnol. **11**, 247 (2016).

[28] T. Ilias, D. Yang, S. F. Huelga, and M. B. Plenio, Criticality-enhanced quantum sensing via continuous measurement, PRX Quantum **3**, 010354 (2022).

[29] S. Gammelmark and K. Mølmer, Fisher information and the quantum Cramér-Rao sensitivity limit of continuous measurements, Phys. Rev. Lett. **112**, 170401 (2014).

[30] M. A. C. Rossi, F. Albarelli, D. Tamascelli, and M. G. Genoni, Noisy quantum metrology enhanced by continuous nondemolition measurement, Phys. Rev. Lett. **125**, 200505 (2020).

[31] F. Albarelli, M. A. C. Rossi, M. G. A. Paris, and M. G. Genoni, Ultimate limits for quantum magnetometry via time-continuous measurements, New J. Phys. **19**, 123011 (2017).

[32] F. Albarelli, M. A. C. Rossi, D. Tamascelli, and M. G. Genoni, Restoring Heisenberg scaling in noisy quantum metrology by monitoring the environment, Quantum **2**, 110 (2018).

[33] A. Cabot, L. S. Muhle, F. Carollo, and I. Lesanovsky, Quantum trajectories of dissipative time crystals, Phys. Rev. A **108**, L041303 (2023).

[34] A. Cabot, F. Carollo, and I. Lesanovsky, Continuous sensing and parameter estimation with the boundary time-crystal, arXiv:2307.13277.

[35] U. Mishra and A. Bayat, Driving enhanced quantum sensing in partially accessible many-body systems, Phys. Rev. Lett. **127**, 080504 (2021).

[36] U. Mishra and A. Bayat, Integrable quantum many-body sensors for ac field sensing, Sci. Rep. **12**, 14760 (2022).

[37] A. S. Holevo, Covariant measurements and imprimitivity systems, in *Quantum Probability and Applications to the Quantum Theory of Irreversible Processes* (Springer, New York, 1984), pp. 153–172.

[38] H. Cramér, *Mathematical Methods of Statistics*, Vol. 26 (Princeton University Press, 1999).

[39] L. M. Le Cam, *Asymptotic Methods in Statistical Decision Theory*, Springer Series in Statistics (Springer, New York, 1986).

[40] C. W. Helstrom, Quantum detection and estimation theory, J. Stat. Phys. **1**, 231 (1969).

[41] R. Zamir, A proof of the Fisher information inequality via a data processing argument, IEEE Trans. Inf. Theory **44**, 1246 (1998).

[42] P. Busch, G. Cassinelli, and P. J. Lahti, On the quantum theory of sequential measurements, Found. Phys. **20**, 757 (1990).

[43] H.-J. Schmidt and J. Gemmer, Sequential measurements and entropy, J. Phys.: Conf. Ser. **1638**, 012007 (2020).

[44] M. Ban, On sequential measurements with indefinite causal order, Phys. Lett. A **403**, 127383 (2021).

[45] B. Skinner, J. Ruhman, and A. Nahum, Measurement-induced phase transitions in the dynamics of entanglement, Phys. Rev. X **9**, 031009 (2019).

[46] M. Block, Y. Bao, S. Choi, E. Altman, and N. Y. Yao, Measurement-induced transition in long-range interacting quantum circuits, Phys. Rev. Lett. **128**, 010604 (2022).

[47] T. Benoist, J.-L. Fatras, and C. Pellegrini, Limit theorems for quantum trajectories, Stochastic Processes Appl. **164**, 288 (2023).

[48] E. Haapasalo, T. Heinosaari, and Y. Kuramochi, Saturation of repeated quantum measurements, J. Phys. A: Math. Theor. **49**, 33LT01 (2016).

[49] T. Benoist, M. Fraas, Y. Pautrat, and C. Pellegrini, Invariant measure for quantum trajectories, Probab. Theory Relat. Fields **174**, 307 (2019).

[50] D. K. Burgarth, P. Facchi, V. Giovannetti, H. Nakazato, S. Pascazio, and K. Yuasa, Exponential rise of dynamical complexity in quantum computing through projections, Nat. Commun. **5**, 5173 (2014).

[51] S. Pouyandeh, F. Shahbazi, and A. Bayat, Measurement-induced dynamics for spin-chain quantum communication and its application for optical lattices, Phys. Rev. A **90**, 012337 (2014).

[52] A. Bayat, B. Alkurtass, P. Sodano, H. Johannesson, and S. Bose, Measurement quench in many-body systems, Phys. Rev. Lett. **121**, 030601 (2018).

[53] W.-L. Ma, P. Wang, W.-H. Leong, and R.-B. Liu, Phase transitions in sequential weak measurements, Phys. Rev. A **98**, 012117 (2018).

[54] T. Rybár and M. Ziman, Process estimation in the presence of time-invariant memory effects, Phys. Rev. A **92**, 042315 (2015).

[55] H. Mabuchi, Dynamical identification of open quantum systems, Quantum Semiclass. Opt. **8**, 1103 (1996).

[56] D. Burgarth, V. Giovannetti, A. N. Kato, and K. Yuasa, Quantum estimation via sequential measurements, New J. Phys. **17**, 113055 (2015).

[57] A. De Pasquale, K. Yuasa, and V. Giovannetti, Estimating temperature via sequential measurements, Phys. Rev. A **96**, 012316 (2017).

[58] A. Ritboon, L. Slodička, and R. Filip, Sequential phonon measurements of atomic motion, Quantum Sci. Technol. **7**, 015023 (2022).

[59] M. Bompais and N. H. Amini, On asymptotic stability of non-demolition quantum trajectories with measurement imperfections, arXiv:2304.02462 [quant-ph].

[60] M. Bompais, N. H. Amini, and C. Pellegrini, Parameter estimation for quantum trajectories: Convergence result, in *2022 IEEE 61st Conference on Decision and Control (CDC)* (IEEE, Piscataway, NJ, 2022), pp. 5161–5166.

[61] S. Gherardini, A. Smirne, M. M. Müller, and F. Caruso, Advances in sequential measurement and control of open quantum systems, Proceedings **12**, 11 (2019).

[62] J. Gambetta and H. M. Wiseman, State and dynamical parameter estimation for open quantum systems, Phys. Rev. A **64**, 042105 (2001).

[63] M. M. Müller, S. Gherardini, A. Smerzi, and F. Caruso, Fisher information from stochastic quantum measurements, Phys. Rev. A **94**, 042322 (2016).

[64] E. Nagali, S. Felicetti, P.-L. de Assis, V. D'Ambrosio, R. Filip, and F. Sciarrino, Testing sequential quantum measurements: How can maximal knowledge be extracted?, Sci. Rep. **2**, 443 (2012).

[65] A. H. Kiilerich and K. Mølmer, Quantum Zeno effect in parameter estimation, Phys. Rev. A **92**, 032124 (2015).

[66] L. A. Clark, A. Stokes, and A. Beige, Quantum jump metrology, Phys. Rev. A **99**, 022102 (2019).

[67] V. Montenegro, G. S. Jones, S. Bose, and A. Bayat, Sequential measurements for quantum-enhanced magnetometry in spin chain probes, Phys. Rev. Lett. **129**, 120503 (2022).

[68] M. Radaelli, G. T. Landi, K. Modi, and F. C. Binder, Fisher information of correlated stochastic processes, New J. Phys. **25**, 053037 (2023).

[69] M. A. Nielsen and I. L. Chuang, *Quantum Computation and Quantum Information* (Cambridge University Press, Cambridge, 2000).

[70] B. W. Shore and P. L. Knight, The Jaynes-Cummings model, J. Mod. Opt. **40**, 1195 (1993).

[71] S. Zhou, M. Zhang, J. Preskill, and L. Jiang, Achieving the Heisenberg limit in quantum metrology using quantum error correction, Nat. Commun. **9**, 78 (2018).